MATERIALS CHEMISTRY
FRONTIERS

RESEARCH ARTICLE

View Article Online
View Journal | View Issue

Cite this: *Mater. Chem. Front.*, 2018, **2**, 910

Solid-state fluorescent materials based on coumarin derivatives: polymorphism, stimuli-responsive emission, self-assembly and optical waveguides†

Rong Rong Cui,[a] Yuan Chao Lv,[b] Yong Sheng Zhao,[b] Na Zhao *[a] and Nan Li *[a]

Received 28th December 2017,
Accepted 5th February 2018

DOI: 10.1039/c7qm00617a

rsc.li/frontiers-materials

Solid-state fluorescent materials have attracted a surge of interest in recent years due to their wide applications in the fields of photoelectric devices, memory storage and fluorescent probes. Compared to the synthesis of new molecules, exploring new properties in known molecules is a facile approach to obtain functionalized fluorescent materials. In this report, we systematically explored the solid-state photoluminescence properties and applications of 7-(diethylamino)coumarin-3-aldehyde (**DCA**) and 7-(diethylamino)coumarin-3-carboxylic acid (**DCCA**). Both fluorophores exhibited a special concentration-dependent emission effect. They displayed polymorphism dependent solid-state emission and single crystal analysis revealed that enhanced overlap between neighbouring molecules resulted in a red-shifted emission. Crystal-to-crystal transformation has also been achieved for both **DCA** and **DCCA** by employing an external thermal treatment. In addition, the solid powder of **DCA** and **DCCA** displayed fluorescence response to HCl and NH_3 gas with high sensitivity. Furthermore, 1D micromaterials were assembled for both fluorophores and **DCA** exhibited outstanding optical waveguide behavior.

Introduction

Organic solid-state fluorescent materials have received considerable attention due to their broad range of applications in the fabrication of organic light-emitting diodes (OLEDs), laser dyes, memory storage materials and fluorescent probes.[1–4] Appropriate solid-state fluorescent materials could provide an optimal choice and could be employed to increase the precision, sensitivity and spatial resolution in diverse research areas.[5] Since the photoluminescence properties of many solid-state fluorophores are significantly influenced by their molecular arrangements, there is an increasing interest in the development of functional materials whose emission color can be efficiently tuned by external stimuli through rearrangement of the molecular packing.[6]

Synthesis of fluorescent molecules with structure diversity is the most creative activity in the field of fluorescent materials. However, creativity in functionalized fluorescent materials has often arisen from novel conceptual interpretations of well-established molecules.[7] Compared to the development of new molecules that may suffer from synthesis complexity and property uncertainty, investigating known fluorophores to explore their superior properties and versatile applications is undoubtedly a shortcut strategy to obtain functionalized fluorescent materials. Indeed, many outstanding properties of star fluorescent molecules were dug out after the first report.[8]

Coumarin, one of the most noted organic fluorophores, has been widely and extensively used in both material and biological sciences due to its inherent physicochemical and photophysical characteristics, such as reasonable stability and relative ease of synthesis.[9] However, in comparison with abundant reports about the photoluminescence research of coumarins in solution, investigations of fluorescence properties as well as potential utilization in the solid state are still rare.[10]

Herein, we report on the exploration of the solid-state optical properties and applications of two fluorophores based on an aminocoumarin scaffold, 7-(diethylamino)coumarin-3-aldehyde (**DCA**) and 7-(diethylamino)coumarin-3-carboxylic acid (**DCCA**) (Scheme 1).[11] Both fluorophores displayed special concentration-dependent emission behaviour. Importantly, two types of crystal with varied emission color were obtained for **DCA** and **DCCA**. Subsequent single crystal analysis revealed the origin of this

[a] *Key Laboratory of Macromolecular Science of Shaanxi Province, Key Laboratory of Applied Surface and Colloid Chemistry of Ministry of Education, School of Chemistry & Chemical Engineering, Shaanxi Normal University, Xi'an, 710119, China. E-mail: nzhao@snnu.edu.cn, nli@snnu.edu.cn*

[b] *Key Laboratory of Photochemistry, Institute of Chemistry, Chinese Academy of Sciences, Beijing 100190, China*

† Electronic supplementary information (ESI) available: Synthesis and characterization, optical spectra, and crystal data. CCDC 1557654. For ESI and crystallographic data in CIF or other electronic format see DOI: 10.1039/c7qm00617a

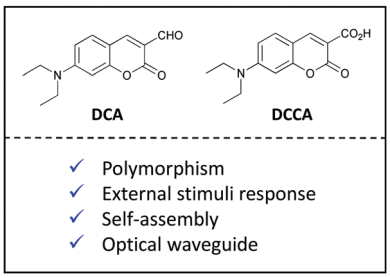

Scheme 1 Chemical structures of **DCA** and **DCCA**.

polymorphism phenomenon. Upon thermal treatment, crystal-to-crystal transformations were achieved for both fluorophores. Meanwhile, the solid state of **DCA** and **DCCA** exhibited sensitive fluorescence response to HCl and NH_3 gas with different modes. Moreover, **DCA** and **DCCA** were able to assemble into 1D micromaterials, while **DCA** possessed remarkable optical waveguide behaviour.

Results and discussion

Concentration-dependent emission

The photophysical properties of **DCA** and **DCCA** were studied in different solvents (Table S1 and Fig. S1, S2, ESI†). The results confirmed their ICT character[12] and **DCCA** exhibited a more pronounced solvatochromic effect due to the stronger electron withdrawing ability of carboxylic acid than aldehyde in the 3-position of coumarin. Interestingly, both fluorophores presented a special concentration-dependent emission effect. As displayed in Fig. 1A, with increasing concentration of **DCA** in THF solution from 1×10^{-6} M to 5×10^{-2} M, a significant bathochromic shift of emission peak (from 470 nm to 520 nm) was observed, while the emission color was changed from light blue to green under 365 nm UV irradiation. Similarly, about 40 nm red-shifted emission was achieved for **DCCA** when the concentration was gradually enhanced from 1×10^{-6} M to 1×10^{-2} M (Fig. 1B). Considering the π-conjugated structure of the coumarin core, the degree of π-overlap could be enhanced by increasing their concentration, which led to relatively larger electronic delocalization and resulted in its red-shifted emission color.[13]

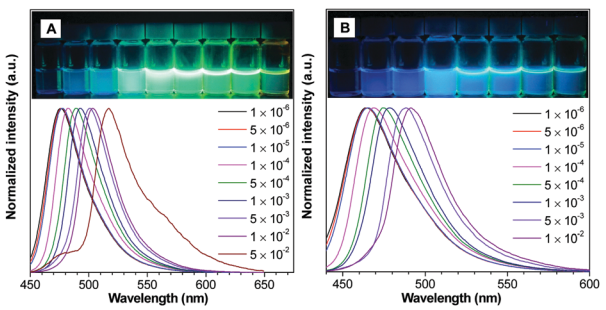

Fig. 1 Normalized PL spectra of **DCA** (A) and **DCCA** (B) in THF at different concentrations. Inset: Photograph of **DCA** (A) and **DCCA** (B) in THF with varied concentrations under 365 nm UV irradiation.

Polymorphism-dependent emission

Since both fluorophores were easy to crystallize, the crystals of **DCA** and **DCCA** were then grown in different solvents. It is worth noting that two plate-like crystals of **DCA** with distinct emission colors were successfully obtained by slowly evaporating their diethyl ether/ethyl acetate and hexane/acetone solution (termed **DCA-Y** and **DCA-R**), respectively. As shown in Fig. 2A–D and Table 1, **DCA-Y** displayed yellow emission at 564 nm with a Φ_F of 7.5% and an average fluorescence lifetime (τ_{avg}) of 8.25 ns, whereas **DCA-R** exhibited red-shifted emission at 602 nm (Φ_F = 7.2%, τ_{avg} = 16.77 ns). It was noted that the corresponding as-prepared powder sample of **DCA** (termed **DCA-P**) gave an orange emission color and the emission spectrum almost overlapped with that of **DCA-Y**, while the Φ_F and τ_{avg} of **DCA-P** were determined to be 7.9% and 5.73 ns, respectively.

Interestingly, two forms of crystals with a nod and plate shape (called **DCCA-G** and **DCCA-R**) were obtained simultaneously by slowly evaporating the dichloromethane/methanol solution of **DCCA** (Fig. 2E–H). A green emission at 518 nm was observed for **DCCA-G** with Φ_F of 9.6% and τ_{avg} of 3.77 ns. In contrast, **DCCA-R** emitted red light at 584 nm (Φ_F = 16.5%, τ_{avg} = 45.13 ns). Different from **DCCA-G** and **DCCA-R**, the as-prepared powder sample of **DCCA** (named **DCCA-P**) displayed the orange emission color (λ_{em} = 573 nm, Φ_F = 8.5%, τ_{avg} = 19.53 ns). It's obvious that both **DCA** and **DCCA** presented significantly polymorphism-dependent emission.[14] Their solid-state emission could be easily tuned by altering the preparation precedures.

PXRD of **DCA** in different states was performed and the results showed that the diffraction profile of **DCA-P** was almost the same as that of **DCA-Y** (Fig. S3A, ESI†), suggesting their similar packing arrangement and almost identical emission. Additionally, the different diffraction pattern of **DCCA** in three states indicated its distinct packing assignment (Fig. S3B, ESI†), which resulted in the distinguishing emission.

To gain further insight into the mechanism of the above pronounced polymorphism properties, single crystal X-ray

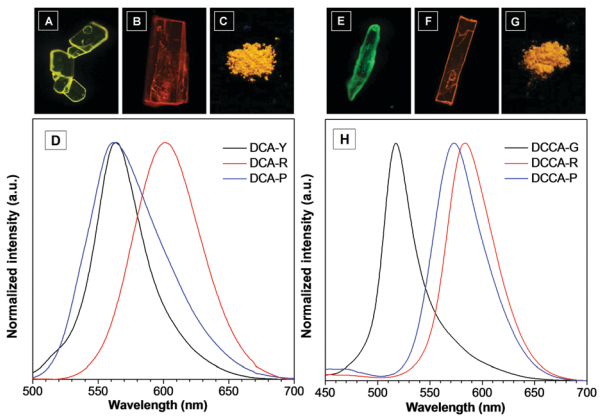

Fig. 2 The photographs of **DCA-Y** (A), **DCA-R** (B) under fluorescence microscopy and **DCA-P** (C) under 365 nm UV irradiation. (D) Normalized PL spectra of **DCA-Y**, **DCA-R** and **DCA-P**. The photographs of **DCCA-G** (E), **DCCA-R** (F) under fluorescence microscopy and **DCCA-P** (G) under 365 nm UV irradiation. (H) Normalized PL spectra of **DCCA-G**, **DCCA-R** and **DCCA-P**.

Table 1 Optical properties of different forms of **DCA** and **DCCA** at 298 K

Compd	λ_{em} [nm]	$\Phi_F{}^a$ (%)	$\tau_{avg}{}^b$ [ns]	k_f [10^9 s^{-1}]	k_{nr} [10^9 s^{-1}]
DCA-Y	564	7.5	8.25	0.009	0.112
DCA-R	601	7.2	16.77	0.004	0.055
DCA-P	562	7.9	5.73	0.014	0.160
DCCA-G	518	9.6	3.77	0.025	0.240
DCCA-R	584	16.5	45.13	0.004	0.018
DCCA-P	573	8.5	19.53	0.004	0.047

[a] Absolute fluorescence quantum yield was measured by using the calibrated integrating sphere system. [b] Average fluorescence lifetime.

structural analysis was carried out and the corresponding crystal data are summarized in Table S2 (ESI†). X-ray diffraction analysis revealed that the molecules in **DCA-Y** adopted a coplanar conformation (Fig. 3A and B) and exhibited a head-to-tail antiparallel packing mode with two types of overlap arrangement (Fig. 3C and D), which resulted in the formation of polymer columns along the *b*-axis direction (Fig. 3E). Within each column, the distances between adjacent molecules were 3.668 Å and 3.515 Å, respectively, suggestive of the strong intermolecular π–π stacking (Fig. 3F). A modest molecular overlap led to a negligible slip angle along the long molecular axis, whereas the slip angle along the short molecular axis was 76.3° (Fig. 3G). Meanwhile, multiple C–H···O (2.524 Å, 2.613 Å and 2.633 Å) interactions existed within the crystal (Fig. S4A, ESI†), which linked columns to form a 3D structure in the crystal.

Although the conformation of the **DCA-R** crystal was similar to that of **DCA-Y** (Fig. 3H), the packing mode was entirely different. In the **DCA-R**, molecules also adopted a head-to-tail antiparallel packing mode (Fig. 3I and J) with two kinds of overlap arrangement, which led to the formation of molecular columns along the *b*-axis (Fig. 3K). The neighbouring molecules in the column also displayed intermolecular π–π stacking (3.396 Å and 3.285 Å) (Fig. 3L). The different molecular overlap in **DCA-R** resulted in a slip angle (59.7°) along the long molecular axis (Fig. 3L), while a very small slip was observed along the short axis (Fig. 3M). Multiple intermolecular C–H···O interactions (2.461 Å, 2.505 Å and 2.520 Å) have also been found throughout the crystal of **DCA-R** (Fig. S4B, ESI†), which hold the columns together in a 3D structure. Compared to the packing of **DCA-Y**, the degree of molecular overlap in **DCA-R** is relatively larger. In addition, **DCA-R** exhibited stronger π–π stacking due to the short distance between neighbouring molecules, which indicated larger electronic excited-state delocalization of **DCA-R** and resulted in its red-shifted emission.

X-ray diffraction analysis revealed that molecules in **DCCA-G** exhibited a coplanar conformation (Fig. 4A and B). In the **DCCA-G**, molecules were in a head-to-head parallel packing mode (Fig. 4C), which resulted in polymer columns along the *a*-axis direction (Fig. 4D). The distance between adjacent molecules in the column was 3.404 Å (Fig. 4E). Meanwhile, the small molecular overlap gave a slip angle of 43.7° along the long molecular axis (Fig. 4E), and the slip angle was 70.0° along the short molecular axis (Fig. 4F). Multiple intermolecular C–H···O interactions (2.659 Å, 2.675 Å and 2.680 Å) have also been found throughout the crystal of **DCCA-G** (Fig. S5A, ESI†), which helped the columns to form a 3D structure.

The conformation of **DCCA-R** was also coplanar (Fig. 4G). Nevertheless, the packing mode in the crystal was very different

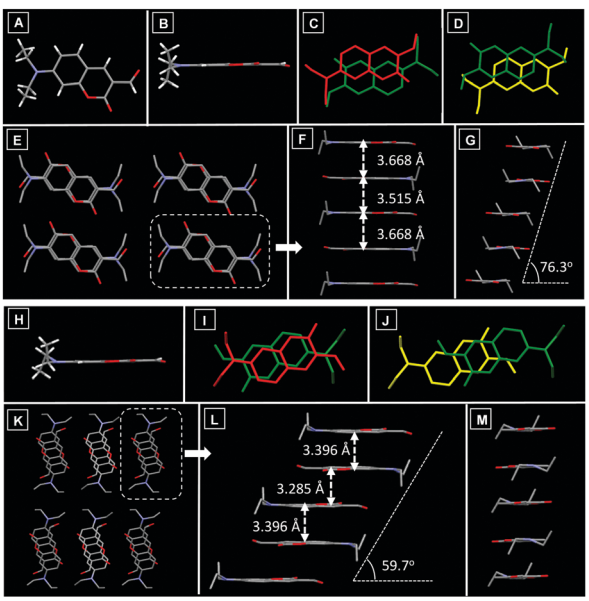

Fig. 3 (A) The molecular conformation of **DCA-Y** in top view. The molecular conformation of **DCA-Y** (B) and **DCA-R** (H) in side view. The molecular overlap between adjacent molecules in **DCA-Y** (C and D) and **DCA-R** (I and J). Molecular stacking structures of **DCA-Y** (E) and **DCA-R** (K) along the *b*-axis. Molecular stacking structures of **DCA-Y** (F) and **DCA-R** (L) along the long molecular axis. Molecular stacking structures of **DCA-Y** (G) and **DCA-R** (M) along the short molecular axis.

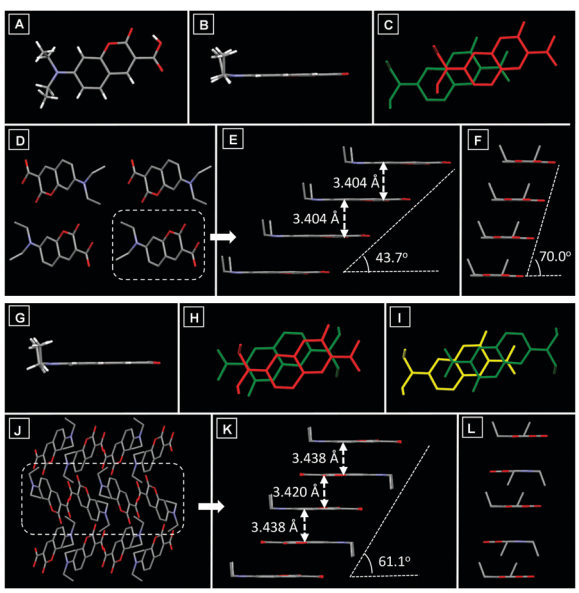

Fig. 4 (A) The molecular conformation of **DCCA-G** in top view. The molecular conformation of **DCCA-G** (B) and **DCCA-R** (G) in side view. The molecular overlap between adjacent molecules in **DCCA-G** (C) and **DCCA-R** (H and I). Molecular stacking structures of **DCCA-G** (D) and **DCCA-R** (J) along the *a*-axis. Molecular stacking structures of **DCCA-G** (E) and **DCCA-R** (K) along the long molecular axis. Molecular stacking structures of **DCCA-G** (F) and **DCCA-R** (L) along the short molecular axis.

from that of **DCCA-G**. When viewed along the *a*-axis, the molecules in **DCCA-R** packed into a 1D chain along the *c*-axis direction (Fig. 4J), which adopted a head-to-tail parallel packing pattern (Fig. 4H and I) with two types of overlap arrangement. The distances between adjacent molecules were 3.438 Å and 3.420 Å (Fig. 4K). The higher degree of molecular overlap led to a larger slip angle (61.1°) along the long molecular axis (Fig. 4K), while there was a very small slip along the short molecular axis (Fig. 4L). Different from **DCCA-G**, multiple C–H···O interactions (2.460 Å, 2.515 Å and 2.630 Å) existed throughout the crystal (Fig. S5B, ESI†), which held the chains in a 3D structure and helped to rigidify the molecular conformation. Upon carefully checking the crystal packing it was revealed that the distance of π–π stacking interactions in **DCCA-G** and **DCCA-R** was similar, but the molecular overlap degree in **DCCA-R** was higher than that in **DCCA-G**. This feature led to the relatively larger electronic delocalization in **DCCA-R** and thus it achieved a bathochromic-shift emission.

Tunable solid-state emission under external stimuli

Both **DCA** and **DCCA** presented intriguing crystal-to-crystal transformation under thermal stimuli. As shown in Fig. 5A, **DCA-Y** displayed an attractive yellow emission color (λ_{em} = 564 nm). However, upon heating at 90 °C for ~2 minutes, the yellow emissive crystal quickly changed into a reddish emissive crystal. Meanwhile, the emission peak of the heated crystal (λ_{em} = 600 nm) overlapped fairly well with the emission profile of **DCA-R** (Fig. S6B, ESI†). A similar phenomenon was achieved for **DCCA-G**. After heating at 110 °C for ~2 minutes, the original green emissive crystal turned into a red emissive one (λ_{em} = 584 nm), and the emission spectrum of the heated sample was almost the same as that of **DCCA-R** (Fig. 5D and Fig. S6D, ESI†). It's noteworthy that the emission color of both heated crystals could not change back at the ambient temperature, which fetched them a potential application in the fabrication of thermographic recording materials. As shown in Fig. 5B and E, the XRD analysis indicated that thermally treated **DCA-Y** and **DCCA-G** possessed good crystallinity and the profiles were similar to those of **DCA-R** and **DCCA-R**, respectively. The above results confirmed the existence of a crystal-to-crystal transformation.[15]

Such crystal-to-crystal conversion was also investigated using differential scanning calorimetry (DSC). As seen in Fig. 5C, two types of crystal (**DCA-Y** and **DCA-R**) gave consistent melting points at 167 °C. During the process of heating, **DCA-Y** displayed a distinct exothermic peak at approximately 87 °C, whereas no peak was detected for **DCA-R**. Combining the emission change, this exothermic peak could be attributed to the thermal phase transition from **DCA-Y** to the thermodynamically stable state of **DCA-R**. The same melting point at 230 °C was observed for crystals of **DCCA-G** and **DCCA-R** (Fig. 5F). However, **DCCA-G** exhibited an exothermic peak at about 105 °C but not **DCCA-R**, suggesting that **DCCA-G** experienced a phase transition to the relatively stable state of **DCCA-R**.

The solid-state emission of **DCA** and **DCCA** could also be tuned by fuming with HCl and NH_3 gas. As shown in Fig. 6A and B, the powder of **DCA** emitted an intense orange emission at 560 nm. However, upon exposing to HCl gas for ~2 minutes, the fluorescence was completely quenched. After being fumed with NH_3 gas for a few minutes, the sample gave a red emission color and the emission peak appeared at 600 nm, which red-shifted by about 50 nm compared with the initial sample of **DCA**. This "off–on" emission switch could be repeated by fuming HCl–NH_3 gas. In sharp contrast, a different phenomenon was found for **DCCA** under the same conditions (Fig. 6C and D). When **DCCA** powder was fumed with HCl gas, the emission color was converted from orange to blue, and the emission peak shifted

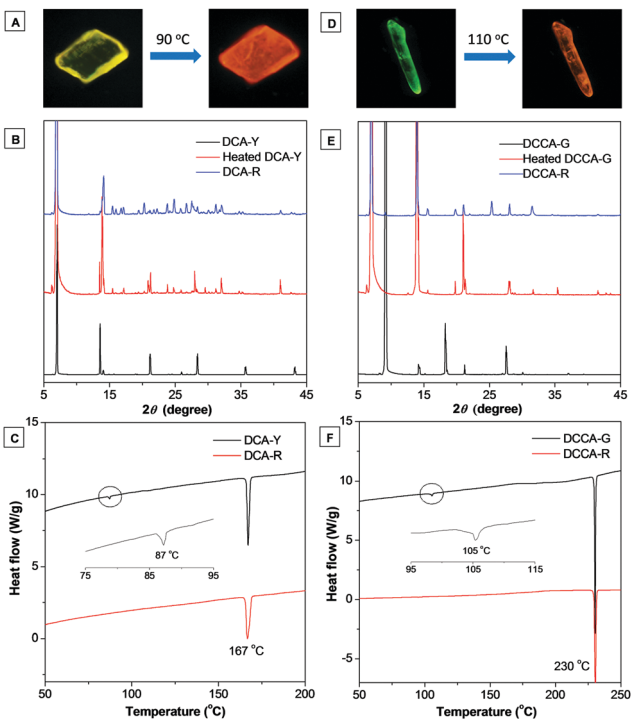

Fig. 5 The photographs of crystal-to-crystal transformation of (A) **DCA-Y** into **DCA-R** and (D) **DCCA-G** into **DCCA-R** under fluorescence microscopy. The XRD patterns of (B) **DCA-Y**, heat-treated **DCA-Y**, **DCA-R** and (E) **DCCA-G**, heat-treated **DCCA-G**, **DCCA-R**. The DSC curves of (C) **DCA-Y**, **DCA-R** and (F) **DCCA-G**, **DCCA-R**.

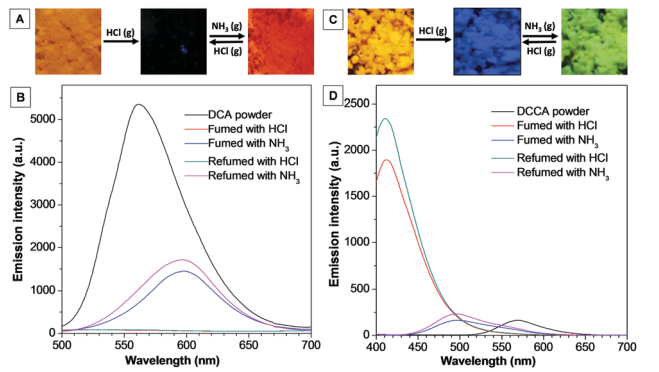

Fig. 6 The fluorescence response of **DCA** and **DCCA** towards HCl and NH_3 gas. Photographs of **DCA** (A) and **DCCA** (B) before and after the treatment with HCl and NH_3 gas under 365 nm UV irradiation. Corresponding PL spectra of **DCA** (C) and **DCCA** (D).

from 570 nm to 420 nm. Subsequently, treating the sample with NH_3 gas brought about a green emission peaked at 500 nm. The emission color between blue and green could be repeated by using HCl–NH_3 gas. The above results confirmed that **DCA** and **DCCA** can be employed as a fluorescent sensor for HCl and NH_3 gas with high sensitivity.

In order to understand the mechanism of the above fluorescence response, ^{1}H NMR analysis of **DCA** and **DCCA** at different states was performed. As shown in Fig. S7 (ESI†), **DCA** possessed a typical aldehyde proton signal at 10 ppm. After the treatment with HCl gas, however, the aldehyde proton disappeared and the signal of aromatic proton shifted significantly. This suggested that both amino and aldehyde groups of **DCA** could undergo a protonation process in an acidic environment. The protonated structure destroyed the ICT process and led to the quenching of fluorescence. The aldehyde proton signal was not recovered after the treatment with NH_3 gas, which could be ascribed to the reaction between NH_3 and the aldehyde group under acidic conditions to give the imine species. The resulting product exhibited stronger ICT character and gave a red-shifted emission compared to its initial state. For **DCCA**, fuming with HCl gas shifted all proton signals down field except for those of the methyl group, suggesting that the protonation of the amino group occurred (Fig. S8, ESI†). As a result, the ICT process was decreased and remarkable blue-shifted emission was observed. After being treated with NH_3 gas, the carboxylic acid group might be ionized due to the neutralization which reduced the ICT effect. Consequently, the green emission was observed.

The above results confirmed that the solid-state emission of **DCA** and **DCCA** could be efficiently tuned by various external stimuli including heating and fuming with acidic or basic gas. In particular for **DCCA**, a considerably wide range of emission was achieved (from 420 nm to 584 nm), which is extremely rare in previous reports about tunable organic solid-state emitters.

Self-assemblies and optical waveguides

Based on crystal analysis, the π–π stacking combined with multiple non-covalent interactions made the two fluorophores capable of self-assembling into ordered structures. Thus, the two fluorophores were employed to fabricate organic micromaterials by using the classic reprecipitation method.[16] By rapidly injecting a specific amount of **DCA** or **DCCA** in THF solution into an ultrasonic aqueous solution and aging the mixture for several hours, floc aggregates were generated. As shown in Fig. 7, fluorescence microscopy and scanning electron microscopy (SEM) images indicated that ordered 1D microrods and microfibers were assembled for **DCA** and **DCCA**, respectively, while the length of these micromaterials was up to 100 μm. Different from the blue light of the two fluorophores in diluted THF solution, yellow (**DCA**, λ_{em} = 555 nm) and orange (**DCCA**, λ_{em} = 570 nm) emission colors were achieved for their micromaterials (Fig. S9, ESI†).

According to the fluorescence microscopy images, bright emission spots at both ends of the micromaterials, while a relatively weak emission from the body, implied that the micromaterials might exhibit optical waveguide behaviour.[17] In order to prove such properties, a distance-dependent fluorescence

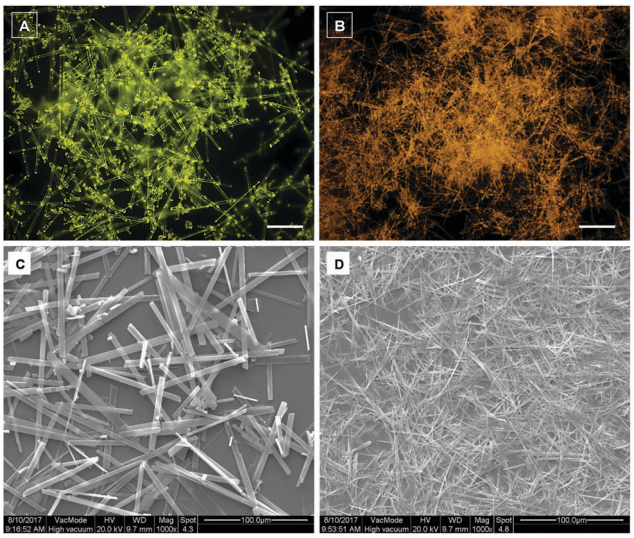

Fig. 7 Fluorescence microscopy and SEM images of **DCA** (A and C) and **DCCA** (B and D) micromaterials. Scale bar in A and B: 20 μm.

image of a single microrod (**DCA**) was taken using a near-field scanning optical microscope. As shown in Fig. 8A, the chosen microrod was excited using a focused laser at six different positions along its length. Obviously, a yellow emission was observed at the end of the rod except for the excited sites. This phenomenon indicated that the microrod propagated the light to the end of the rod, indicative of the optical waveguide behaviour. The emission spectra were collected in the fixed emitting ends with varied excitation positions (labelled with 1–6) (Fig. 8B). The results showed that the emission intensity was decreased with increasing distance between the excited site and the

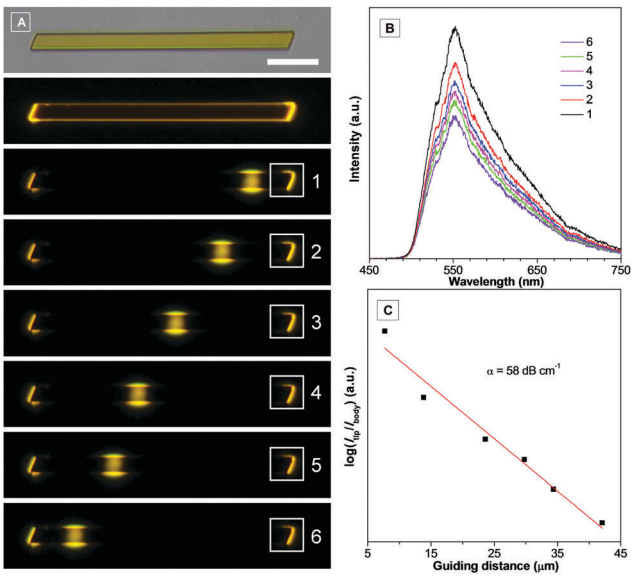

Fig. 8 (A) Fluorescence micrographs obtained by exciting an identical **DCA** microrod at different positions. Corresponding emission spectra of the emitting ends labelled with numbers 1–6 in (B). (C) Fitted plot of $\log(I_{end}/I_{body})$ *versus* the distance (x) between the excited site and the emitting end. Scale bar: 10 μm.

emitted end, which originated from the optical loss during the propagation process. The emission intensities (550 nm) at the fixed end (I_{end}) and the excited site (I_{body}) were recorded, and the optical loss coefficient (a) was calculated by using the equation $\log(I_{end}/I_{body}) = -\alpha x$, where x is the distance between the excited site and emitting end (Fig. 8C). The α value of **DCA** was determined to be 58 dB cm^{-1}, which was quite low compared with previous reports.[6c,15b,17a,18] The well-ordered arrangement of microrods as well as their smooth surface should be responsible for such excellent optical waveguide behaviour.

Conclusions

In summary, multiple solid-state fluorescence properties were explored in two fluorophores that were derived from aminocoumarin (**DCA** and **DCCA**). Both fluorophores exhibited typical solvent and concentration-dependent emission effects. Importantly, they displayed a remarkable polymorphism phenomenon with tunable solid-state emission, which was attributed to their diverse molecular packing mode. In addition, crystal-to-crystal transformations were achieved for both fluorophores by thermal treatment. Meanwhile, the emission of the solid powder could be tuned efficiently by HCl and NH_3 gas. Moreover, both **DCA** and **DCCA** assembled into ordered 1D micromaterials, and **DCA** gave excellent optical waveguide properties. These unique features endowed both fluorophores with broad potential applications in fields of optical recording, pH sensing and photoelectric devices. The strategy of exploring new properties in known molecular systems also provides an ideal way to construct multifunctional organic solid fluorophores.

Conflicts of interest

There are no conflicts to declare.

Acknowledgements

We are grateful for financial support from the National Natural Science Foundation of China (21672135, 21402115 and 51403122), the Fundamental Research Funds for the Central Universities (GK201703024 and GK201702002) and the Natural Science Foundation of Shaanxi Province (2016JQ2020).

Notes and references

1 (*a*) Z. Y. Yang, Z. Mao, Z. L. Xie, Y. Zhang, S. W. Liu, J. Zhao, J. R. Xu, Z. G. Chi and M. P. Aldredb, *Chem. Soc. Rev.*, 2017, **46**, 915–1016; (*b*) M. C. Gather, A. Köhnen and K. Meerholz, *Adv. Mater.*, 2011, **23**, 233–248; (*c*) M. R. Zhu and C. L. Yang, *Chem. Soc. Rev.*, 2013, **42**, 4963–4976; (*d*) M. Stępień, E. Gońka, M. Żyła and N. Sprutta, *Chem. Rev.*, 2017, **117**, 3479–3716.

2 (*a*) A. J. C. Kuehne and M. C. Gather, *Chem. Rev.*, 2016, **116**, 12823–12864; (*b*) I. D. W. Samuel and G. A. Turnbull, *Chem. Rev.*, 2007, **107**, 1272–1295.

3 (*a*) B. Cho, S. Song, Y. Ji, T. W. Kim and T. Lee, *Adv. Funct. Mater.*, 2011, **21**, 2806–2829; (*b*) H. L. Dong, H. F. Zhu, Q. Meng, X. Gong and W. P. Hu, *Chem. Soc. Rev.*, 2012, **41**, 1754–1808.

4 (*a*) L. Basabe-Desmonts, D. N. Reinhoudt and M. Crego-Calama, *Chem. Soc. Rev.*, 2007, **36**, 993–1017; (*b*) V. S. Padalkar and S. Seki, *Chem. Soc. Rev.*, 2016, **45**, 169–202; (*c*) C. Ge, Y. Liu, X. Ye, X. Zheng, Q. Han, J. Liu and X. Tao, *Mater. Chem. Front.*, 2017, **1**, 530–537.

5 (*a*) S. J. Yoon, J. W. Chung, J. Gierschner, K. S. Kim, M. G. Choi, D. H. Kim and S. Y. Park, *J. Am. Chem. Soc.*, 2010, **132**, 1367–13683; (*b*) Y. N. Hong, J. W. Y. Lam and B. Z. Tang, *Chem. Commun.*, 2009, 4332–4353; (*c*) H. Sasabe and J. Kido, *Chem. Mater.*, 2011, **23**, 621–630; (*d*) D. Yan and D. Evans, *Mater. Horiz.*, 2014, **1**, 46–57; (*e*) Z. J. Zhao, B. R. He and B. Z. Tang, *Chem. Sci.*, 2015, **6**, 5347–5365.

6 (*a*) Y. Sagara, S. Yamane, M. Mitani, C. Weder and T. Kato, *Adv. Mater.*, 2016, **28**, 1073–1095; (*b*) T. Seki, T. Ozaki, T. Okura, K. Asakura, A. Sakon, H. Uekusa and H. Ito, *Chem. Sci.*, 2015, **6**, 2187–2195; (*c*) P. Z. Chen, H. Zhang, L. Y. Niu, Y. Zhang, Y. Z. Chen, H. B. Fu and Q. Z. Yang, *Adv. Funct. Mater.*, 2017, **27**, 1700332; (*d*) K. Wang, H. Zhang, S. Chen, G. Yang, J. Zhang, W. Tian, Z. Su and Y. Wang, *Adv. Mater.*, 2014, **26**, 6168–6173; (*e*) P. Galer, R. C. Korošec, M. Vidmar and B. Šket, *J. Am. Chem. Soc.*, 2014, **136**, 7383–7394; (*f*) C. Wang and Z. Li, *Mater. Chem. Front.*, 2017, **1**, 2174–2194; (*g*) H. Naito, Y. Morisaki and Y. Chujo, *Angew. Chem., Int. Ed.*, 2015, **54**, 5084–5087; (*h*) W. A. Morris, T. Butler, M. Kolpaczynskaa and C. L. Fraser, *Mater. Chem. Front.*, 2017, **1**, 158–166.

7 (*a*) G. Ulrich, R. Ziessel and A. Harriman, *Angew. Chem., Int. Ed.*, 2008, **47**, 1184–1201; (*b*) R. W. Sinkeldam, N. J. Greco and Y. Tor, *Chem. Rev.*, 2010, **110**, 2579–2619.

8 (*a*) J. D. Luo, Z. L. Xie, J. W. Y. Lam, L. Cheng, H. Y. Chen, C. F. Qiu, H. S. Kwok, X. W. Zhan, Y. Q. Liu, Y. Q. Liu, D. B. Zhu and B. Z. Tang, *Chem. Commun.*, 2001, 1740–1741; (*b*) J. Mei, N. L. C. Leung, R. T. K. Kwok, J. W. Y. Lam and B. Z. Tang, *Chem. Rev.*, 2015, **115**, 11718–11940; (*c*) D. Ding, K. Li, B. Liu and B. Z. Tang, *Acc. Chem. Res.*, 2013, **46**, 2441–2453.

9 (*a*) F. G. Medina, J. G. Marrero, M. Macías-Alonso, M. C. González, I. Córdova-Guerrero, A. G. T. Garcíaa and S. Osegueda-Roblesa, *Nat. Prod. Rep.*, 2015, **32**, 1472–1507; (*b*) J. Liu, Y. Q. Sun, Y. Y. Huo, H. X. Zhang, L. F. Wang, P. Zhang, D. Song, Y. W. Shi and W. Guo, *J. Am. Chem. Soc.*, 2014, **136**, 574–577; (*c*) Z. S. Wang, Y. Cui, K. Hara, Y. Dan-oh, C. Kasada and A. Shinpo, *Adv. Mater.*, 2007, **19**, 1138–1141; (*d*) M. E. Riveiro, N. De Kimpe, A. Moglioni, R. Vazquez, F. Monczor, C. Shayo and C. Davio, *Curr. Med. Chem.*, 2010, **17**, 1325–1338; (*e*) M. Tasior, D. Kim, S. Singha, M. Krzeszewski, K. H. Ahn and D. T. Gryko, *J. Mater. Chem. C*, 2015, **3**, 1421–1446.

10 (*a*) C. T. Chen, C. L. Chiang, Y. C. Lin, L. H. Chan, C. Huang, Z. W. Tsai and C. T. Chen, *Org. Lett.*, 2003, **5**, 1261–1264; (*b*) M. R. Shreykar and N. Sekar, *Dyes Pigm.*, 2017, **142**, 121–125; (*c*) U. Venkataramudu, M. Annadhasan, H. Maddali

and R. Chandrasekar, *J. Mater. Chem. C*, 2017, **5**, 7262–7269; (*d*) F. Bu, R. Duan, Y. Xie, Y. Yi, Q. Peng, R. Hu, A. Qin, Z. Zhao and B. Z. Tang, *Angew. Chem., Int. Ed.*, 2015, **54**, 14492–14497; (*e*) H. Yan, X. Meng, B. Li, S. Ge and Y. Lu, *Dyes Pigm.*, 2017, **146**, 479–490; (*f*) S. Kumar, P. Singh, R. Srivastava, R. R. Koner, A. Pramanik, J. Mathew, S. Sinha, M. Rawat, R. S. Anande and S. Ghosh, *J. Mater. Chem. C*, 2014, **2**, 6637–6647; (*g*) H. Moon, Q. P. Xuan, D. Kim, Y. Kim, J. W. Park, C. H. Lee, H. J. Kim, A. Kawamata, S. Y. Park and K. H. Ahn, *Cryst. Growth Des.*, 2014, **14**, 6613–6619; (*h*) B. Ventura, Y. M. Poronik, I. Deperasińska and D. T. Gryko, *Chem. – Eur. J.*, 2016, **22**, 15380–15388.

11 (*a*) M. Cigan, J. Donovalova, V. Szocs, J. Gasper, K. Jakusova and A. Gaplovsky, *J. Phys. Chem. A*, 2013, **117**, 4870–4883; (*b*) X. C. Li, L. Yang, X. W. Zhang, L. F. Li, Y. Zhou and Y. A. Son, *Z. Kristallogr. – New Cryst. Struct.*, 2014, **229**, 241–242; (*c*) R. Arcos-Ramos, M. Maldonado-Domínguez, J. Ordóñze-Hernández, M. Romero-Ávila, N. Farfán and M. D. P. Carreón-Castro, *J. Mol. Struct.*, 2017, **1130**, 914–921; (*d*) H. Zhang, T. Z. Yu, Y. L. Zhao, D. W. Fan, L. L. Chen, Y. Q. Qiu, L. Qian, K. Zhang and C. H. Yang, *Spectrochim. Acta, Part A*, 2008, **69**, 1136–1139; (*e*) X. G. Liu, J. M. Cole, P. C. Y. Chow, L. Zhang, Y. Z. Tan and T. Zhao, *J. Phys. Chem. C*, 2014, **118**, 13042–13051.

12 (*a*) B. Raju and T. S. Varadarajan, *J. Phys. Chem.*, 1994, **98**, 8903–8905; (*b*) A. Chatterjee and D. Seth, *Photochem. Photobiol.*, 2013, **89**, 280–293; (*c*) K. S. Hettie and T. E. Glass, *Chem. – Eur. J.*, 2014, **20**, 17488–17499; (*d*) A. Chatterjee, B. Maity and D. Seth, *Phys. Chem. Chem. Phys.*, 2013, **15**, 1894–1906.

13 H. Yu, W. Ren, H. Lu, Y. Liang and Q. Wang, *Chem. Commun.*, 2016, **52**, 7387–7389.

14 (*a*) H. Pan, P. Liu, Y. Li, Y. Wu, B. S. Ong, S. Zhu and G. Xu, *Adv. Mater.*, 2007, **19**, 3240–3243; (*b*) C. Näther and I. Jeβ, *Angew. Chem., Int. Ed.*, 2006, **45**, 6381–6383; (*c*) R. H. Li, S. Z. Xiao, Y. Li, Q. F. Lin, R. H. Zhang, J. Zhao, C. Y. Yang, K. Zou, D. S. Li and T. Yi, *Chem. Sci.*, 2014, **5**, 3922–3928; (*d*) G. Q. Zhang, J. W. Lu, M. Sabat and C. L. Fraser, *J. Am. Chem. Soc.*, 2010, **132**, 2160–2162; (*e*) J. N. Zhang, H. Kang, N. Li, S. M. Zhou, H. M. Sun, S. W. Yin, N. Zhao and B. Z. Tang, *Chem. Sci.*, 2017, **8**, 577–582.

15 (*a*) T. H. Kim, Y. W. Shin, J. H. Jung, J. S. Kim and J. Kim, *Angew. Chem., Int. Ed.*, 2008, **47**, 685–688; (*b*) X. Gu, J. Yao, G. Zhang, Y. Yan, C. Zhang, Q. Peng, Q. Liao, Y. Wu, Z. Xu, Y. Zhao, H. Fu and D. Zhang, *Adv. Funct. Mater.*, 2012, **22**, 4862–4872.

16 Y. Zhao, X. Mu, C. Bao, Y. Fan, J. Zhang and Y. Wang, *Langmuir*, 2009, **25**, 3264–3270.

17 (*a*) Y. S. Zhao, J. J. Xu, A. D. Peng, H. B. Fu, Y. Ma, L. Jiang and J. N. Yao, *Angew. Chem., Int. Ed.*, 2008, **47**, 7301–7305; (*b*) N. Zhao, M. Li, Y. l. Yan, J. W. Y. Lam, Y. L. Zhang, Y. S. Zhao, K. S. Wong and B. Z. Tang, *J. Mater. Chem. C*, 2013, **1**, 4640–4646.

18 (*a*) C. Shi, Z. Guo, Y. Yan, S. Zhu, Y. Xie, Y. S. Zhao, W. Zhu and H. Tian, *ACS Appl. Mater. Interfaces*, 2013, **5**, 192–198; (*b*) S. Chen, N. Chen, Y. L. Yan, T. Liu, Y. Yu, Y. Li, H. Liu, Y. S. Zhao and Y. Li, *Chem. Commun.*, 2012, **48**, 9011–9013.

